Paleolimnological reconstruction of the centennial eutrophication processes in a sub-tropical South American reservoir

Article *in* Journal of South American Earth Sciences · June 2020

DOI: 10.1016/j.jsames.2020.102707

CITATIONS
0

READS
158

8 authors, including:

Silvana Halac
Centro de Investigaciones en Ciencias de la Tierra
11 PUBLICATIONS **281** CITATIONS
SEE PROFILE

Luciana Mengo
National University of Cordoba, Argentina
1 PUBLICATION **0** CITATIONS
SEE PROFILE

Lucia Guerra
University of Chile
13 PUBLICATIONS **64** CITATIONS
SEE PROFILE

Andrea Lami
Italian National Research Council
139 PUBLICATIONS **2,780** CITATIONS
SEE PROFILE

Paleolimnological reconstruction of the centennial eutrophication processes in a sub-tropical South American reservoir

S. Halac[1*], L. Mengo[1], L. Guerra [1,2,3], A. Lami [4], S. Musazzi [4], J.-L. Loizeau[5], D. Ariztegui[2], E.L. Piovano[1]

Abstract
Reservoirs hold a detailed record of the changes in the input of sediments and nutrients over decades to centuries. Paleolimnological multi-proxy analysis makes it possible to reconstruct baseline conditions to infer early evidence of environmental change. Our study aims to reconstruct historical human impacts derived from urban development on the San Roque reservoir (Córdoba, Argentina) related to the centennial dynamics of sedimentary and eutrophication processes.
A paleolimnological record, dated by ^{210}Pb and ^{137}Cs, made it possible to identify two stages during the environmental evolution of the San Roque reservoir. Physical processes, such as fluvial discharge and water level variation, dominantly ruled stage 1 (Unit C) during the initial infilling of the reservoir. Nutrient load and eutrophication processes controlled stage 2 (Units B and A). Stage 1 (77-55 cm; AD 1921 to 1965) occurred before and after the second dam was built and while the level of water increased by ≈8 m; it displayed a high variation in mean grain size and maximum values of magnetic susceptibility. Stage 2 (AD 1965–2017) records a new reservoir base level and the maintenance of high water levels and comparatively more stable conditions.
Regarding the eutrophication process throughout stage 2, three sub-stages were defined: a) Sub-stage I (AD 1965–1985) is a period of incipient eutrophication; b) Sub-stage II (AD 1985–2005) is an interval of increase of eutrophication as shown by the increase in several organic proxies related to the abundance of phytoplankton. Echinenone, zeaxanthin and myxoxanthophyll indicate that cyanobacteria increased concentration by three-to four-fold in comparison with the previous sub-stage. c) Sub-stage III (AD 2005–2017) shows the transition to a hypereutrophic state. Diatomea (*fuco* and *diato*), dinophyceae (*diadino*), chlorophyta (*lut*) and cryptophyta (*allo*) groups show a comparatively higher contribution.
Our results mostly highlight that during the last century the main drivers of changes in the environmental state of the San Roque reservoir were trophic, fluvial and hydrometeorological. These results might provide tools for anticipating future scenarios for water management plans under increasing anthropic pressure.

Keywords
Central Argentina; San Roque reservoir; Trophic state; Fossil pigment; Anthropocene

[1] *Centro de Investigaciones en Ciencias de la Tierra (CICTERRA), Consejo Nacional de Investigaciones Científicas y Técnicas (CONICET)-Universidad Nacional de Córdoba (UNC), Avenida Vélez Sarsfield 1699, (X5016) Córdoba, Argentina*
[2] *Department of Earth sciences, University of Geneva, rue des Maraichers 13, 1205 Geneva, Switzerland*
[3] *Núcleo Milenio Paleoclima. Universidad de Chile, Facultad de Ciencias, Las Palmeras 3425, Ñuñoa, Santiago de Chile, Chile*
[4] *Istituto di Ricerca sulle Acque (IRSA-VB), sede di Verbania, Consiglio Nazionale delle Ricerche (CNR), Largo Tonolli 50, 28922 Verbania Pallanza, Italy*
[5] *Department F.-A. Forel for Environmental and Aquatic Sciences, University of Geneva, 66 Boulevard Carl-Vogt, CH-1211 Geneva 4, Switzerland*
*__Corresponding author__: silvana.halac@unc.edu.ar, srhalac@gmail.com (S. Halac).

1. Introduction

Paleolimnological studies in Southern South America have focused mostly on climate reconstructions since lakes contain high resolution records of the Last Glacial-to-interglacial transition and Holocene (see references in Piovano et al., 2014). However, the growing concern about the pollution of aquatic systems as a major threat to both humans and freshwater biodiversity (Vörösmarty et al., 2010) created a new challenge for palaeolimnology in the study of lakes and reservoirs to provide tools to ensure water quality. Although reservoir sediments were scarcely considered as environmental archives,

the need to track changes in water quality, before monitoring, pinpoints the value of reservoir sedimentary records in deciphering anthropic-derived environmental changes (Bradbury and Van Metre, 1997; Shotbolt et al.,2006; Tremblay et al., 2001; Winston et al., 2014).

Aquatic systems are threatened on a world-wide scale by a variety of pollutants as well as the negative impacts of land-use or water management practices; as a consequence, eutrophication of lakes and reservoirs has become a global problem over the last decades (Smith, 2003). Eutrophication is a natural process that is accelerated by human activities in aquatic systems and relates to the increased loading of key nutrients, phosphorus and nitrogen, from domestic, agricultural or industrial sources. This environmental problem has caused not only the deterioration of water quality but also major changes in the biological community structure (Smith and Schindler, 2009). Many studies in aquatic systems within diverse geological and geographical settings show that climate-driven processes can act synergistically with the anthropic influence, increasing, for instance, lake primary productivity and therefore changes in the system's trophic state and water quality (O'Neil et al., 2012; Paerl and Huisman, 2008; Paerl and Paul, 2012). Consequently, a pressing need for evaluation of trends in water quality has arisen in order to provide tools for action based on knowledge (Bartram and Ballance, 1996).

Although reliable monitoring data are crucial for such assessments, available databases are not long enough to fully encompass the environmental evolution from pre-disturbance levels to the present. In order to substitute the lack of historical data, paleolimnological proxies provide unique information to reconstruct changes in water quality, trophic state, sedimentary processes and land-use, among others. Since a complex network of interactions governs lake ecosystems, a multi-proxy approach is necessary to better unravel past changes (Birks and Birks, 2006; Smol, 2010). Among the existing proxy-data to reconstruct past trophic state and primary productivity, fossil pigments can be used as indicators of algal and bacterial community composition (Leavitt and Hodgson, 2001; Buchaca and Catalan, 2007; Lami et al., 2010). Biochemical remains of photosynthetic organisms (carotenoids, chlorophylls, photoprotective compounds and other lipid-soluble molecules) are unique indicators to infer the temporal dynamic of phytoplankton groups (Reuss et al., 2005). Fossil pigments provide reliable information to track historical changes of abundance and composition of the phytoplankton communities and can be considered indices of present and past lake trophic conditions and climate changes (Coianiz et al., 2014; Huo et al., 2019). One of the most common fossil pigments preserved in the sedimentary record in all phototrophic organisms is chlorophyll *a* – and its derivatives, frequently used as indicators of total phytoplankton biomass. Carotenoids however, comprising carotene and xanthophylls, are preferentially preserved in the sedimentary record because they are more stable than chlorophylls. β-carotene, which is present in all phytoplankton taxa, has been recognized as a biological tracer for total phototrophic quantification and thus provides a reliable indicator of paleoproductivity (Leavitt, 1993; Romero-Viana et al., 2009).

Our study, based on a centennial multi-proxy analysis of the San Roque reservoir (SRr, Argentina), addresses some aspects related to the temporal dynamics of sedimentary and eutrophication processes and associated changes in the composition of the phytoplankton community. The SRr is located in the central semi-arid region of Argentina, which is characterized by the presence of a high number of reservoirs due to water scarcity. Over recent decades, the water quality of these reservoirs has deteriorated significantly, especially due to eutrophication (O'Farrell et al., 2019). A generalized problem is the lack of continuous water quality monitoring surveys, which have only started 20 years ago. Consequently, a main difficulty in assessing the current state is the lack of knowledge of their pre-disturbance environmental conditions during periods of low anthropic impact and the identification of early evidence of change. Despite the importance of reservoirs as sources of water supply, few paleolimnological studies tackling trophic state changes related to anthropic and natural forces have been conducted in South America (Costa-Böddeker et al., 2012; Fontana et al., 2014; Gangi et al., 2020).

Our reconstruction aims to infer paleolimnological conditions of SRr, especially prior to the beginning of water quality monitoring in AD 1999. The study focuses on answering some unresolved questions: (1) How many stages can be recognized in the history of the SRr through changes in physical, chemical and biological proxies? (2) How are these stages related to environmental processes and eutrophication? (3) What is the response of the phytoplankton community throughout the environmental history of the SRr?

This study constitutes one of the first attempts to investigate environmental changes in reservoirs in the semiarid region of Argentina from a paleolimnological perspective and intends to provide an assessment for the development of water management tools.

2. Study site, limnology, regional climate and land use

The SRr (31°22' S, 64°27' W) is a reservoir located in a semi-arid region of Argentina at 608 m a.s.l. in the upper basin of the Suquía River (Fig. 1). A first dam was built between AD 1881 and 1891 with a maximum height of 29 m, which at that moment was the largest dam in the world. A subsequent dam of 35.3 m in height was built between AD 1939 and 1944, enlarging the capacity of the reservoir from 112 to 201 hm^3 (Ballester, 1931). Nowadays the reservoir is used for different purposes such as urban water supply, flood control, power generation, minor irrigation, recreation and tourism. The SRr supplies drinking water to approximately one million people in the Córdoba city area. The drainage area is 1750 km^2 while the reservoir has a surface of $\approx$15 km^2 and mean water depth of $\approx$ 13 m, resulting in a volume of 201 hm^3. The maximum water-depth is 35 m and is located at

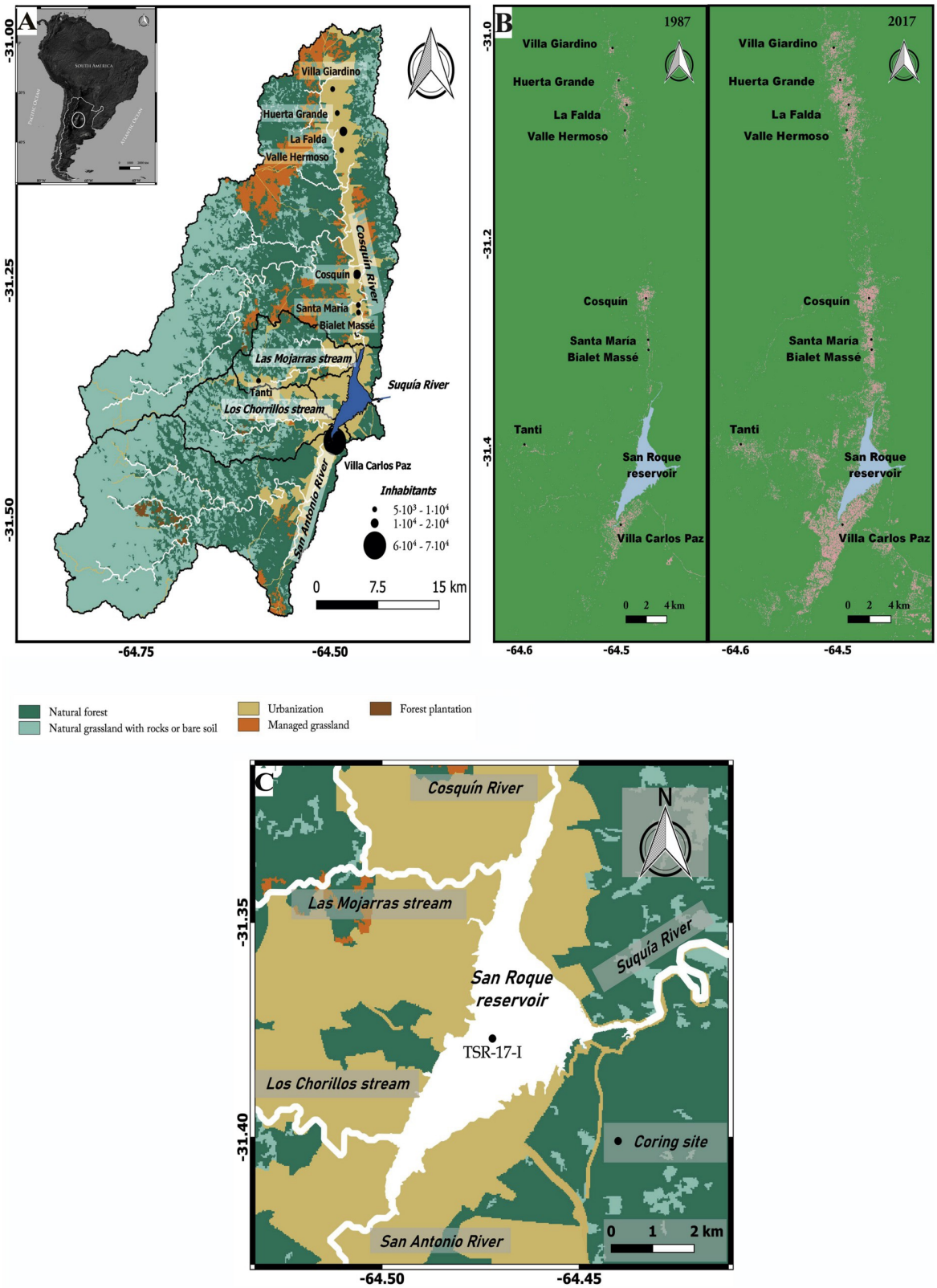

Figure 1. A) San Roque reservoir location in South America and in central Argentina. SRr catchment land uses, main localities and inhabitants (census 2010). B) Spatiotemporal urban growth in the San Roque reservoir catchment area based on the multi-temporal analysis of Landsat 5 (1987) and Landsat 8 (2017) satellites images. C) Detailed map of San Roque reservoir showing the coring site indicated as TSR-17-I. Land uses, main tributaries and the outlet river are indicated.

the dam area. The Cosquín and San Antonio rivers and Las Mojarras and Los Chorrillos streams are the main tributaries, while the Suquía River is the outlet (Fig. 1B and C), (Dasso et al., 2014; Granero et al., 2004). Today the reservoir is a warm monomictic lake, frequently stratified during the austral summer season (December to February). The mean residence time of the water is 0.6 years. General features of the SRr are presented in Table 1.

The regional climate condition is semihumid to semiarid. Mild temperatures, summer-concentrated rainfall, and occasional snowfall in winter are typical features. Local mean annual temperature is 14°C witha wide monthly variation range: minimum mean value of 7°C and maximum mean value of 24°C (Table 1). Rainfall regimes regulate the discharge of the tributary rivers. The mean annual precipitation is 780 mm. More than 80% of the annual rainfall occurs between October and April (Colladón, 2014). Interannual precipitation analysis reports drought cycles of about 10 years, alternating with wet periods of 10 years. This pattern changed after the 1980s, when droughts become less severe (Díaz et al., 2016). The latter is related to a hyper-humid interval that occurred from the mid-1970s to 2005, due to a regional hydroclimatic change (Pasquini et al., 2006; Piovano et al., 2014; Guerra et al., 2017).

Catchment land use (Fig. 1A) shows a high urban influence, while some areas are partially modified by managed grassland for breeding cattle, however they are not extensive activities. Intense urban development without adequate infrastructure and planning is largely transforming the catchment. Thus, the main source of pollution is represented by human domestic waste (mainly bacteria and nutrients) as the SRr receives untreated sewage discharges from direct and diffuse sources (Halac et al., 2019). In addition, deforestation and fire cause frequent loss of soil and vegetation in the watershed, increasing the eutrophication process (Rodríguez and Ruiz, 2016). Tourism represents the main activity within the area. Several localities are located within the catchment but Villa Carlos Paz, sited at the lake shore, is the largest with 6.3 x 10^4 permanent inhabitants (Fig. 1A; https://datosestadistica.cba.gov.ar/dataset/censo-2010-resultados-definitivos) and increasing to ≈30 x 10^4 during the summer season (https://datosestadistica.cba.gov.ar/dataset/sector-turismo). Satellite images show the urban expansion along the catchment from 1987 to 2017, revealing that Villa Carlos Paz city is the area of major growth, followed by other localities located at the north of the catchment, mainly Cosquín and La Falda (Fig. 1B).

According to some scattered limnological studies, the first report claiming for eutrophication of the SRr goes back to the 1970s (Bonetto et al., 1976) whereas recently (*ca*. 2012), the trophic state of the SRr was reported to have become hypereutrophic (Rodríguez and Ruiz, 2016). During the last decade, nutrients mean content of soluble reactive phosphorus, total phosphorus and total inorganic nitrogen has been 24, 83 and 385 $\mu g \cdot L^{-1}$ respectively and mean chlorophyll a content has been around 51 $\mu g \cdot L^{-1}$ (Table 1). Cyanobacteria blooms were first signaled in 1963 (Pizzolon et al., 1999) and have become a more frequent event since the 1980s (Quirós, 1988). Because of increasing eutrophication, today the SRr presents frequent hypolimnetic anoxia, dominance of cyanobacteria (mainly *Microcystis aeruginosa* and *Dolichospermum spp.*), and fish death events (Rodríguez and Ruiz, 2016).

Regular monitoring of reservoir water quality started only after 1999, providing information about physical, chemical and biological water column variables (Table 1). However, there is an information gap regarding limnological conditions during the first *ca*. 100 years of dam operation. Hence, paleolimnological reconstruction may be the only tool available to reveal the dynamic of some processes that occurred at the SRr since the first dam was built.

3. Material and Methods

3.1 Core sampling, description and methods

A 77-cm-long sediment core (TSR-17-I) was retrieved in September 2017, using a gravity corer (IQTEC, "Bob corer type"). The core was collected in the central area of the reservoir (31°22' 35.95" S; 64°28' 12.60" W; Fig. 1C), at a water depth of 17 m. The core was stored at 4°C within 1-2 h after collection.

Whole-core petrophysical properties were determined on TSR-17-I core. Computer tomography images made it possible to recognize fine-scaled sedimentary structures in the undisturbed sedimentary core. The core was cut in two halves and photographed. An initial description of the core was made following the criteria proposed by the Limnological Research Center Core Facility (http://lrc.geo.umn.edu/laccore/icd.html). Laminated ($\leq$1 cm), banded ($>$1 cm) and massive sediments, as well as textural and color changes were visually identified. Magnetic susceptibility was measured using a MS2E Bartington sensor every 0.5 cm, at the Paleolimnology Laboratory, IRSA-VB, Pallanza, Italy. Sediment sampling was performed every 1 cm or at a lithological and/or magnetic susceptibility change.

The mean grain size was determined using a laser diffraction grain size analyzer (HORIBA LA-950) at GeoLab - CICTERRA, Argentina. Samples were pre-treated with 20 mL of 30% H_2O_2 to eliminate the organic matter, and with 20 mL HCl (10%) to remove carbonates. Sediments were subsequently rinsed with distilled water and the residue was dispersed with a solution of 10 mL of $(NaPO_3)_6$ to defloculate particles. Mean grain size and textural classes were determined in metric units using the Gradistat software (Blott and Pye, 2001).

Water content was calculated by weighing subsamples before and after drying at 105°C for 24 hours. Organic matter (OM) was determined by loss-on-ignition (LOI). Samples were heated at 550°C for 2 hours to remove organic matter, re-weighed and then heated at 950°C for 2 h, and again weighed (Dean, 1974; Heiri et al., 2001). Mass loss (percentage of dry weight) after combustion at 550°C (LOI 550°C) is

Table 1. Physicochemical characteristics of San Roque reservoir. For physicochemical variables related to quality water, only the values of the center area of the reservoir, where the core was obtained, are presented (expressed as mean and standard deviation).

San Roque reservoir	Lat. S 31°22'; Long. W 64°27'
Reservoir area / volume[1]	15 km^2 / 201 hm^3
Reservoir watershed area[1]	1750 km^2
Tributaries area[1]	Cosquín river: 827 km^2 / Las Mojarras stream: 89 km^2 San Antonio river: 515 km^2/ Los Chorrillos stream: 138 km^2
Depth[2]	Maximum: 35.3 m; average: 13 m
Average water residence time[2]	≈ 0.1-0.7 yr
Mixing regime[3]	Warm monomictic (with frequent stratification during summer)
Trophic state[3]	Hypereutrophic
pH[3]	7.9 ± 0.72
Dissolved oxygen[3]	9.5 ± 4.3 $mg{\cdot}L^{-1}$
Secchi disk[3]	1.2 ± 0.35 m
Phosphorous[3]	Total: 83 ± 67 $\mu g{\cdot}L^{-1}$, reactive soluble: 24 ± 15 $\mu g{\cdot}L^{-1}$
Nitrogen[3]	Dissolved inorganic: 385 ± 210 $\mu g{\cdot}L^{-1}$
Chlorophyll*a*[3]	51 ± 80 $\mu g{\cdot}L^{-1}$
Mean air temperature[4]	Annual: 14°C; winter: 7°C; summer: 24°C
Mean annual precipitation[4,5]	780 mm

[1]Dasso et al., 2014; [2]Granero et al., 2004;[3]Rodríguez and Ruiz, 2016;[4]Colladón, 2014;[5]Díaz et al., 2016.

proportional to the amount of organic matter.

3.2 Chronology

^{210}Pb and ^{137}Cs activity profiles were obtained using a HPGe well gamma spectrometer (Ortec EG&G) measuring gamma emissions at 46.5 keV and 662 keV respectively, at the Department F.-A. Forel of the University of Geneva, Switzerland. ^{210}Pb and ^{137}Cs activity was measured on 1 cm-thick samples of dried, powdered and homogenized sediments collected with a 7 cm interval for the entire core. Around the maximum ^{137}Cs peak, additional samples with 3 cm intervals were measured to better define the peak.

Prior to ^{210}Pb analysis, samples were sealed to prevent any loss of ^{222}Rn and stored for a period of 3 weeks to ensure secular equilibrium between ^{226}Ra and ^{214}Pb. Excess ^{210}Pb was calculated as the difference between total ^{210}Pb and the supported ^{210}Pb determined by ^{214}Pb measurement (Appleby, 2001). The detection efficiency of the radioisotopes was corrected for geometry, density and chemical composition using Monte Carlo simulation software (Gespecor 4.1, Sima et al., 2001). Corrections were substantial for ^{210}Pb (up to 25% change), but not for ^{137}Cs (about 1-2%).

^{210}Pb ages for the Core TSR-17-I were calculated considering the Constant Rate of Supply model (CRS, Appleby, 2001; Robbins, 1978). Mass accumulation rates (MAR, $g{\cdot}cm^{-2}{\cdot}yr^{-1}$) were calculated using sediment dry density (Sanchez-Cabeza et al., 2012). The radioactive fallout from nuclear weapon tests in the atmosphere (Pennington et al., 1973) was used as the marker to test the ^{210}Pb chronological model. The main regional ^{137}Cs peak at sites located at latitude 30-40 south of the Equator correspond to AD 1964 while the first detection for ^{137}Cs at the same location is AD 1955 (Leslie and Hancock, 2008; UNSCEAR, 2000).

3.3 Pigment and elemental analysis

Pigment measurements and elemental analysis were performed on samples taken at 1 cm intervals at the Paleolimnology Laboratory, IRSA-VB, Pallanza, Italy.

For elemental analysis, the sediments were dried, homogenized and ground in an agate mortar prior to elemental analysis. Total carbon (C_{tot}) and total nitrogen (N_{tot}) were analyzed via high temperature combustion on a CHNS analyzer (Fisons NA1500). Duplicate analyses of every sample were run, and the mean of the two measurements are reported here. Replicate analysis of one sample (n= 5) gave a precision of ± 0.02 wt % C_{tot} and ± 0.003 wt % N_{tot}.

Fossil pigments were determined according to the method described by Lami et al., (1994) on subsamples kept frozen until laboratory analysis. About 2 g of wet sediment were taken three weeks after core extraction, weighed and extracted overnight with ≈ 5 mL of acetone/water mixture (90:10), under nitrogen atmosphere and maintained at 4°C in darkness. The extract was then centrifuged at 4000 rpm for 10 min and used for chlorophyll and carotenoid determinations. Total fossil pigments (chlorophylls and their derivatives, CD; total carotenoids, TC) were measured spectrophotometrically (SAFAS, mod. $UVmc^2$) in a 1 cm light path cuvette. The extracts were read at 410, 430, 450, 665 and 750 nm. CD were calculated as spectrophotometer units per gram organic matter $U{\cdot}\ (g\ LOI)^{-1}$ as described by Guilizzoni et al., (1983), and TC were calculated as $mg{\cdot}\ (g\ LOI)^{-1}$ following Züllig (1985). CD and TC are expressed in terms of organic matter

content to reflect the degree of pigment preservation relative to that of the total organic matrix in which the pigment occurs (Hodgson et al., 2004).

Individual carotenoids and chlorophylls were detected by Reversed Phase High-Performance Liquid Chromatography at 460 and 656 nm respectively, using an UltiMate 3000, ThermoFisher (Lami et al., 1994). The HPLC system consists of an autosampler (Ultimate 3000), a quaternary pump (P680), a thermostated column oven (TCC100) and a DAD detector (Ultimate 3000). The column is a C18 ODS (Omnispher 5 µm particle size; 250 mm x 4.6 mm ID). The chromatogram was acquired at 460 nm and 656 nm for carotenoids and chlorophyll pigments, respectively. The whole spectrum for peak identification was also recorded. After sample injection (100 µL of acetone extract), a gradient program that ramped from 85% mobile-phase A (80:20, by vol. methanol: aqueous solution of 0.001 M PIC A ion-pairing and 0.001 M propionic acid) to 100% mobile-phase B (60:40, acetone: methanol) in 30 min with a hold for 20 min provided sufficient resolution of all pigments of interest. Flow rates from 1 mL min^{-1} to 2 mL· min^{-1}. The column was re-equilibrated between samples by linear ramping to 85% mobile-phase A for 5 min and maintained for 10 min before sample injection. With this procedure, we were able to separate zeaxanthin from lutein and β-carotene from pheophytin *a*. Analysis of replicates of sediment samples yielded a CV of 4.5% - 11.5%, depending on the pigments. Identification of all pigments was confirmed by comparison of spectral characteristics and chromatographic mobility of pigments isolated from sediments with those obtained from: TLC analysis (Züllig, 1982), commercial standards (DHI Laboratory Products, Denmark) and published values (Egeland et al., 2011). Concentrations of pigments were determined on the basis of molar extinction coefficients at the detection wavelengths. The molar extinction coefficient E1% 460 and E1% 656 was derived from the E1% max reported in Egeland et al. (2011). The pigment affiliation was based on Guilizzoni and Lami (2003).

3.4 Statistical analysis

A multivariate technique was used for ordination on physicochemical and biological proxies over the sediment record. A preliminary detrended correspondence analysis (DCA) was performed to identify the most appropriate analytical method. Principal component analysis (PCA) was applied as a linear response was confirmed (ter Braak, 1995). Temporal trends in organic proxies (OM, C_{tot}, and N_{tot}) and fossil pigments (CD and specific carotenoids markers) were analyzed statistically using the non-parametric Mann–Kendall test (Gilbert, 1987). Statistical analysis were performed with the Vegan package (Oksanen et al., 2019; R software) and the Kendall package (McLeod, 2011; R software) for ordination and trend analyses, respectively.

4. Results

4.1 Sedimentary core data

4.1.1 Age model

There is a general decreasing trend in total ^{210}Pb activity due to the decay of the unsupported ^{210}Pb (Fig 2A). ^{210}Pb age model reached a minimum age of AD 1921 at the base of the sediment record (Fig 2A). Overall the sediment record MAR shows two distinctive patterns. A low MAR (0.25 ± 0.04 g·cm^{-2}·yr^{-1}) is estimated between 77 and 56 cm, corresponding to ^{210}Pb dates AD 1921 and 1964, respectively. Comparatively a higher MAR (0.36 ± 0.05 g·cm^{-2}·yr^{-1}) characterizes the uppermost sediments between 49 to 0 cm corresponding to ^{210}Pb dates AD 1966 and 2017. Between sediment depths 55 to 50 cm the ^{210}Pb profile shows fairly constant activity values assigned to AD 1965, highlighting a high sedimentation rate during this period (Fig. 2A).

Signs of ^{137}Cs activity appear at a depth of 60 cm and are attributed to AD 1955, the first hemispheric nuclear weapon detections in sediment profiles of fallout (AD 1954-1957; Leslie and Hancock, 2008). A wide maximum peak from 55 to 51 cm in depth is attributed to the regional fallout peak of AD 1964 (Fig. 2B; Leslie and Hancock, 2008; UNSCEAR, 2000). Based on these time markers, MAR correspond to 0.24 and 0.35 g·cm^{-2}·yr^{-1}, respectively, which are fully compatible with rates determined by ^{210}Pb dating. The large ^{137}Cs peak coincides with the layer showing ^{210}Pb constant activity values, confirming a change in sedimentation rate (Figs. 2 A and B).

Both age models (Fig. 2C) highlight the existence of three sediment dynamic conditions throughout the record: 1) Low MAR from AD 1921 to 1964; 2) a fast sedimentation layer (levels 55 to 50 cm) around AD 1965; and 3) higher MAR from AD 1966 to 2017.

4.1.2 Physicochemical properties and detailed sedimentology

The multi-proxy analysis of the core, including visual inspection of sediments and the response of physicochemical proxies throughout the sequence, made it possible to identify three lithological units from bottom to top: UC, UB and UA (Fig. 3; Table 2).

The lowermost UC consisted of finely laminated and banded light brown coarse silts (77-55 cm; AD 1921 – 1965). It is characterized by the coarsest sediments of the record (mean grain size = 17.3 ± 4.7 µm) including a finning-upward trend at the top of the unit. Magnetic susceptibility values range from a maximum of 715 to 221 SI· 10^{-7}. Organic matter content varies from 11.7 to 13.5% DW while C_{tot} and N_{tot} range from 3.4 to 5.5% DW and from 0.37 to 0.59% DW respectively. The top of UC presents a sharp limit marked by an abrupt interruption of laminated sediments.

Unit B (55-14 cm; AD 1965 – 2005) consists of massive and banded brown medium silts including isolated black laminae. This unit shows comparatively finer grain sizes (12.4 ± 1.0 µm) and lower magnetic susceptibility values (346 SI· 10^{-7}) than UC. Mean grain size shows small variation along UB, ranging from 10.7 to 14.1 µm. UB shows a fining-upward trend

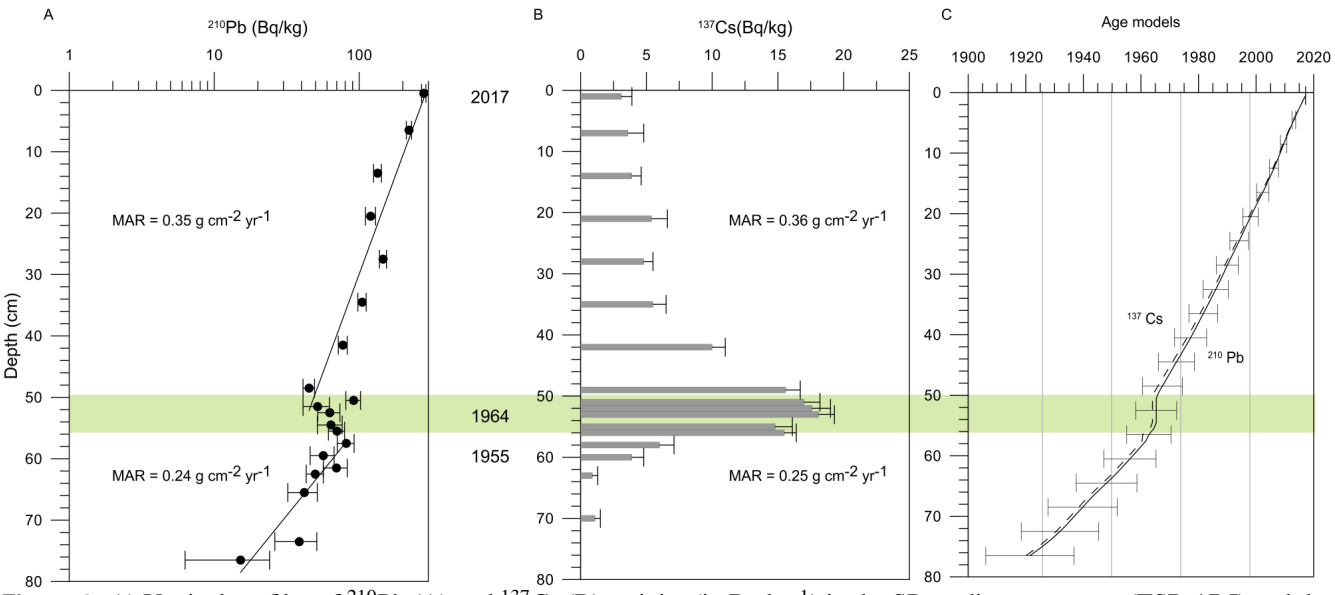

Figure 2. A) Vertical profiles of ^{210}Pb (A) and ^{137}Cs (B) activity (in Bq kg^{-1}) in the SRr sedimentary core (TSR-17-I) and the respective mass accumulation rates (MAR). Dates of both beginning and maximum of ^{137}Cs atmospheric fallout are indicated. C) Age ^{210}Pb and ^{137}Cs models obtained from the MARs calculated for each interval with different sedimentation patterns: 77 to 56 cm and 49 to 0 cm. ^{210}Pb model uncertainties are shown by error bars.

along the top of the unit (level 15 cm; 11.1 µm). Magnetic susceptibility shows a decreasing trend reaching a minimum value at the top of the unit (135 SI·10^{-7}). OM, C_{tot} and N_{tot} mean values are 12.5 ± 0.3, 3.8 ± 0.2 and 0.44 ± 0.02% DW, respectively, while a slight increase is observed above level 33 cm (AD 1985) matching with the development of thin dark laminated sediments.

UA (14 cm - 0 cm; AD 2005 – 2017) is recognized by the presence of a faintly laminated interval at the base of the unit and a jelly-like consistency layer at the top. The base of UA is characterized by a pronounced geochemical shift, evident through a noticeable rising in OM content towards the top of the core (mean value: 14.0 ± 0.7% DW; maximum value: 15.7% DW). C_{tot} and N_{tot} contents also show an upward increase to maximum values of 5.7 and 0.63% DW respectively. The unit presents low values of magnetic susceptibility (279 SI·10^{-7}) and a mean grain size of 12.0 ± 1.7 µm.

4.1.3 Fossil pigment proxies

Figures 4 and 5 summarize fossil pigment concentration from AD 1921 to 2017. Even though fossil pigments vary greatly throughout the core, most of them display a synchronous increase towards the top of the sequence.

Chlorophyll derivatives (CD) and total carotene (TC) profiles show a similar pattern throughout UC and UB. Along UA their behavior is different, especially at the uppermost levels (above 6.5 cm), where CD displays a sharp and steady rise. Conversely, TC displays fairly constant values in UA and UB (Fig. 4). The noticeable increase in CD pigments at the uppermost part of the sedimentary core corresponds to both a rise in chlorophyll *a* (maximum value 150 nmol. g LOI^{-1}) and to a significant contribution of the chlorophyll *a* degradation product: pheophytin *a* (phe *a*), pheophorbide *a* (pheide *a*) and chlorophyllide *a* (maximum values: 194, 468 and 176 nmol. g LOI^{-1}, respectively). Contents of β-carotenes ($\beta\beta$-car) exhibit large variations along UC followed by a marked decrease in the first part of UB (55 to 33 cm). The upper part of UB (33 to 14 cm) and the entire UA are characterized by a shift to larger and steadier values.

Regarding the specific pigment markers of each phytoplankton group (Fig. 5; Electronic Supplementary Material Table A1), one of the most frequent assemblages along the entire sedimentary sequence is echinenone (*echin*) and zeaxanthin (*zea*), characteristics of cyanobacteria group. Myxoxanthophyll (*myxo*) and canthaxanthin (*cantha*) are also cyanobacteria pigment indicators; the former is representative of colonial cyanobacteria whereas the latter is typical of N_2 fixers. *Myxo* and *cantha* exhibit a similar trend to *echin*. Higher concentrations are observable within the upper section of UC (i.e., 59 to 55 cm; maximum values: 191, 80 and 10 nmol· g LOI^{-1} for *echin*, *myxo* and *cantha*, respectively) which are then followed by a sharp decrease along the lower part of UB. Aphanizophyll (*apha*) pigment, a cyanobacteria marker specific of N_2-fixers, was not detected along Unit C.

At UB, a steady increase above the level 33 cm was identified for *echin*, *zea*, *myxo* and *cantha* (maximum values: 162, 148, 76 and 18 nmol ·g LOI^{-1}, respectively). Regarding *apha*, this marker was continuously detected above 20 cm depth (maximum value: 17 nmol ·g LOI^{-1}). Multiple peaks were detected at UA for *echin*, *zea*, *myxo*, *cantha* and *apha* (from 11 to 6 cm; maximum values: 102, 139, 65, 29 and 9 nmol ·g LOI^{-1}, respectively).

The carotenoid marker for identifying chlorophyta, *i.e.*, lutein

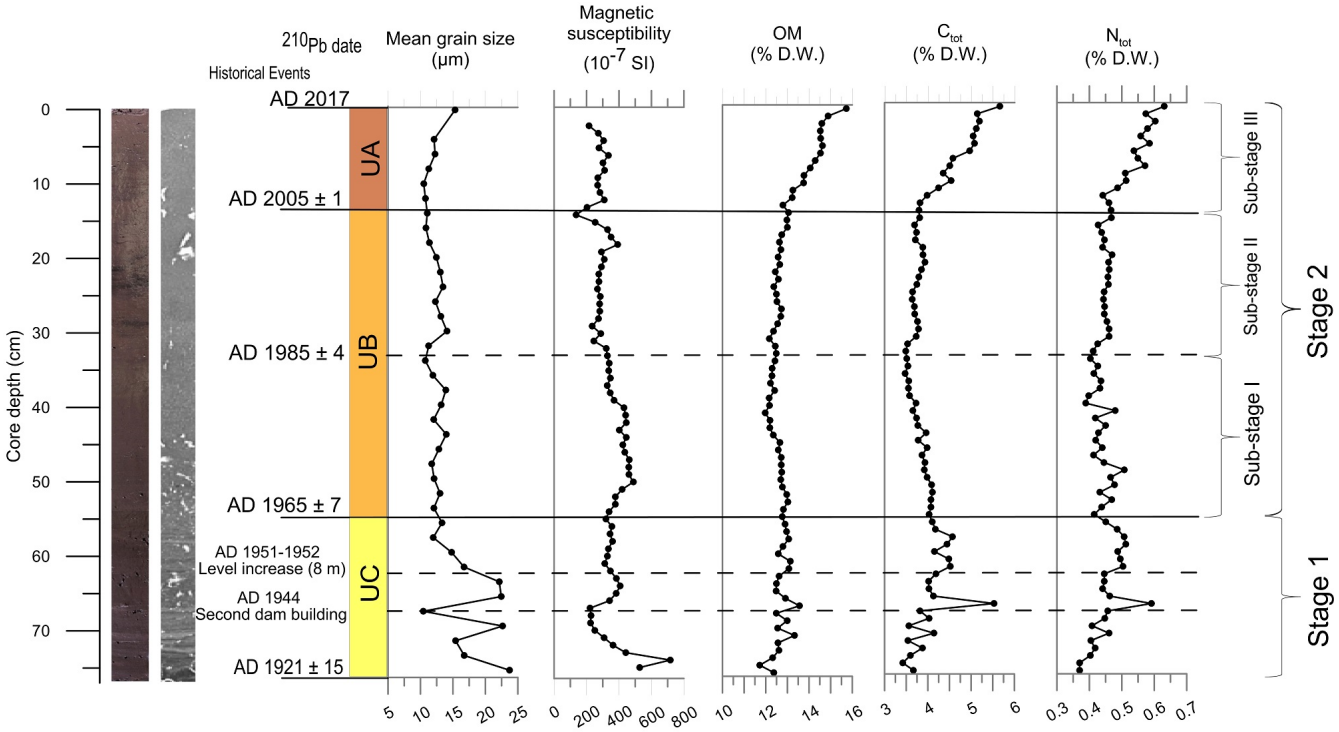

Figure 3. Depth profiles of physicochemical proxies in the SRr sedimentary core (TSR-17-I): mean grain size (MGS, micrometers), magnetic susceptibility (MS, SI units), organic matter (OM, %), total carbon (C_{tot}, %) and total nitrogen (N_{tot}, %). Core photograph and computed tomography image are shown on the left. Lithological units C, B and A are indicated from base to top. Historical events are described along units. San Roque reservoir evolution stages (1 and 2) and sub-stages (I, II and III) are indicated (see discussion section).

(*lut*), displays a sharp peak at UC (70 to 65 cm, 142 nmol ·g LOI^{-1}) and shows high values at UA (11 to 7 cm; maximum value: 143 nmol ·g LOI^{-1}).

Siliceous algae pigment indicators, fucoxanthin (*fuco*) and diatoxanthin (*diato*), display peaks at UC (70 to 67 cm; maximum values: 149 and 105 nmol ·g LOI^{-1}, respectively) and a single peak at UB (level 33: 112 and 64 nmol ·g LOI^{-1}, respectively), and finally UA displays a sharp increase reaching maximum values of 101 and 93 nmol ·g LOI^{-1}, respectively. Diadinoxanthin (*diadino*) used as a dinophyceae indicator presents a relative increase at the uppermost UA (maximum value: 106 nmol ·g LOI^{-1}). Alloxanthin (*allo*), characteristic of the cryptophyte group, exhibits a uniform pattern along UC and UB, showing maximum values at UA (max. value: 170 nmol ·g LOI^{-1}).

4.2 PCA ordination of physicochemical and biological proxies

In order to obtain a comprehensive view of physicochemical and biological proxy fluctuations along the record, we plotted the two main axes of variability obtained from a principal component analysis (PCA; Fig. 6). PCA data show that the two first components account together for more than the 50% of the total variance. The first axis explains the 40.6% of the total variance and might be associated with the trophic state. Cyanobacteria (*echin*, *zea*, *myxo*, *cantha* and *apha*), dinophyceae (*diadino*), cryptophyta (*allo*), chlorophyll derivatives (CD) and organic matter (OM) are positively related with axis 1 while magnetic susceptibility is negatively correlated with fossil pigments. On the other hand, the second axis accounted for 15.1% of variance and might indicate physical process influences. Diatom (*fuco* and *diato*), chlorophyta (*lut*) and mean grain size (MGS) are positively correlated with axis 2. Most of the samples corresponding to Unit C (77 to 55 cm; S1) and the lower part of Unit B (55 to 33 cm; Ss I) are grouped on the left side of the first component. On the other hand, the major proportion of samples corresponding to the uppermost part of UB (Ss II) and UA (Ss III) are on the right-hand side (Fig. 6).

4.3 Hydrometeorological instrumental record

The instrumental record of the reservoir water level and precipitations cover the period AD 1947-2017 (Catalini and García, 2014; Vicario, 2017). The water level curve shows a sharp increase of ≈ 8 m from AD 1951 to 1952 after the building of the second dam (Fig. 7A). Although important short-term water level variability was registered (*i.e.*, a 3 m drop during AD 1964-1965), high water levels were maintained until AD 1969. Afterwards, a water level drop of ≈ 7 m took place until AD 1971 followed by a rise of ≈ 4 m at AD 1972. The record from AD 1972 to the present includes multiple water level fluctuations, but of lesser magnitude than those registered

Table 2. Mean and standard deviation of physical and chemical proxies for each lithological unit. MS: Magnetic Susceptibility; MGS: Mean grain size; OM: Organic Matter; C_{tot}: Total Carbon; N_{tot}: Total Nitrogen

Lithological Units	n	MS (10^{-7} SI)	MGS (μm)	OM (% D.W.)	C_{tot} (% D.W.)	N_{tot} (% D.W.)
C	22	Mean: 357 ± 109 Max: 716 Min: 222	Mean: 17.3 ± 4.7 Max: 23.7 Min: 10.4	Mean:12.7 ± 0.4 Max: 13.5 Min: 11.7	Mean: 4.1 ± 0.4 Max: 5.5 Min: 3.4	Mean: 0.45 ± 0.05 Max: 0.59 Min:0.37
B	41	Mean:346 ± 78 Max: 488 Min: 135	Mean:12.4 ± 1.0 Max: 14.1 Min: 10.7	Mean: 12.5 ± 0.3 Max: 13.1 Min: 12.0	Mean: 3.8 ± 0.2 Max: 4.1 Min: 3.5	Mean: 0.44 ± 0.02 Max: 0.51 Min: 0.39
A	16	Mean: 279 ± 38 Max: 334 Min: 135	Mean: 12.0 ± 1.7 Max: 15.3 Min: 10.5	Mean: 14.0 ± 0.7 Max: 15.7 Min: 12.8	Mean: 4.7± 0.5 Max: 5.7 Min: 3.8	Mean: 0.54 ± 0.05 Max: 0.63 Min: 0.44

during the 1951-1972 interval. The precipitation record over the same period shows a pattern that mostly resembles reservoir water level fluctuations with the exception of the interval corresponding to the reservoir infilling after the building of the second dam (Fig. 7A).

5. Discussion

The high-resolution multi-proxy analysis encompass the environmental evolution and the sedimentary dynamics and eutrophication history from AD 1921 to 2017.

The synchronic correspondence of lithological units, sedimentary organic matter, total C and N content, and fossil pigment made it possible to identify two main reservoir stages. Fluvial-like sedimentary conditions during the initial infilling of the reservoir were followed by an increasing trend in nutrient load, associated to a eutrophication processes typical for inner-lake dominated conditions mainly due to an increase in water level. In general, organic proxies and fossil pigment concentration increased quite synchronously, especially during the last three decades (*e.g.*, OM, tau: 0.767, $p \leq 0.001$; C_{tot}, tau: 0.697, $p \leq 0.001$; N_{tot}, tau: 0.543, $p \leq 0.001$; CD, tau: 0.554, $p \leq 0.001$; *echin+zea+myxo*, tau: 0.314, $p \leq 0.001$; *cantha* + *apha*, tau: 0.508, $p \leq 0.001$; *diadino*, tau: 0.464, $p \leq 0.001$; Figs. 3-5). This fact indicates that the increase in fossil pigments is largely the result of increased internal productivity in the SRr, rather than the effect of differences in the autochthonous / allochthonous OM balance (Lami et al., 2000).

Water physicochemical data collected during the last two decades show that hypoxia or anoxia dominate the lower part of the hypolimnion in the SRr during most of the year, thus preventing the direct photo-oxidation of pigments in the water column during deposition. Fossil pigments generally show good preservation throughout the core as supported by 430 nm: 410 nm ratios (Moss, 1967), which mostly show a range of values from 0.97 to 0.88 (Fig. 4). However, a marked decrease of the 430 nm: 410 nm ratio can be observed throughout the uppermost sediments (0.81 ± 0.2; Fig. 4). Such a change is most evident in the top ≈ 5 cm which are subject to continuous processes of diagenesis (Guilizzoni and Lami, 2003). Hence, the preservation/degradation conditions should be considered when interpreting the SRr record of fossil pigments, especially at uppermost layers.

5.1 SRr's evolution stages

One of the most remarkable outcomes of our multi-proxy analysis of the SRr sedimentary record is the identification of two main stages: one is dominantly ruled by physical processes, such as water level variation (Stage 1), while the other is controlled by changes in the nutrient load (Stage 2) (Figs. 3-7).

The first stage, recorded by finely laminated and banded sediments of UC, spans from AD 1921 to 1965. Stage 1 represents the initial time period after construction of the first dam in AD 1888, as well as the increase in water level after the second dam implementation in AD 1944. UC sediments show a great variation in the mean grain size, displaying coarser sediments and maximum magnetic susceptibility values before the level corresponding to AD 1944. A high fluvial influence, mainly due to the small volume of the reservoir, characterizes the onset of this period. After the building of the second dam, the resulting water level increase by ≈ 8 m can be inferred by the particle-finning trend towards the top of UC. The dominance of comparatively finer sediments can be attributed to changes in the transport dynamics of fluvial sediments due to a rise in the base level. Previous limnological studies in the SRr (Guarrera, 1948) reported an influx of riverine phytoplankton species into the reservoir, remarking the high riverine influence during this stage.

The second stage (UB + UA) is the record of increased water level reservoir conditions, after the second dam became operative together with comparatively lower water level fluctuations (Fig. 7A). Changes in lake morphometry and longer distances to river mouth control sediment load transport resulting in a decrease of mean grain size and the accumulation of massive sediments. These conditions probably weakened the riverine influence and promoted lentic sedimentary conditions, especially in the central area of the reservoir.

During the second stage we did distinguish three sub-stages related to the eutrophication process and with marked shifts in fossil pigment composition and concentration (Figs. 4 and 5). Sub-stage I is represented by the basal section of UB (55

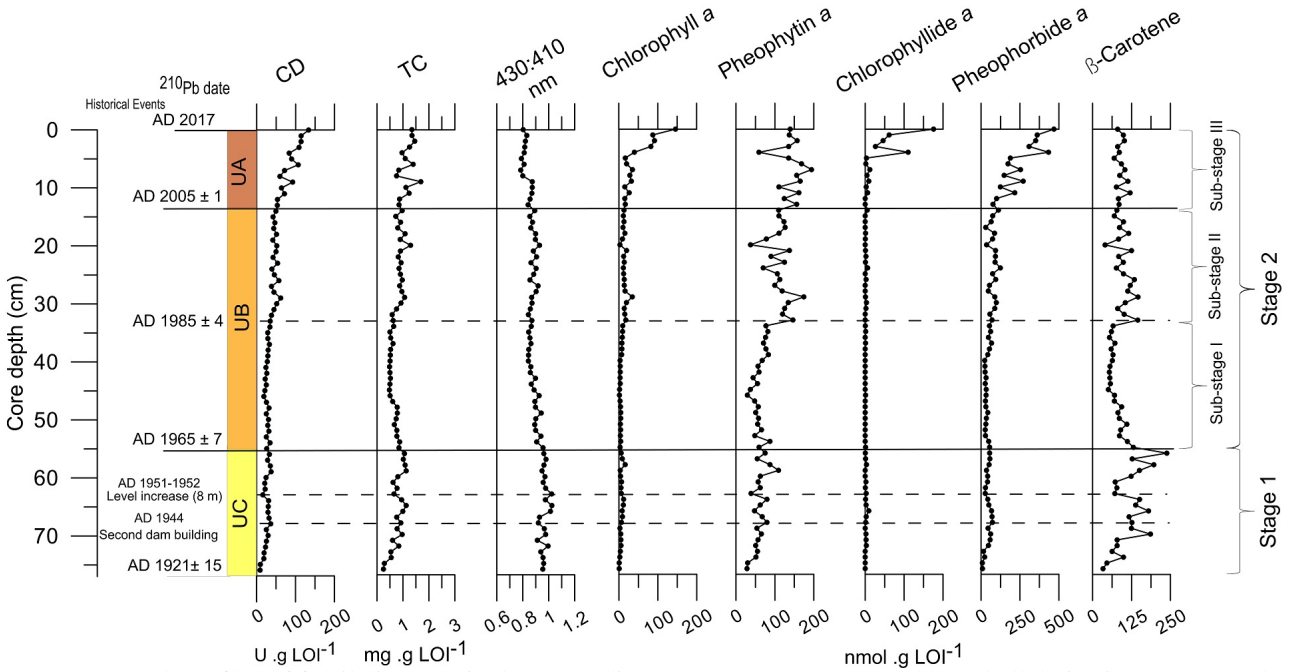

Figure 4. Depth profiles of fossil pigments in the SRr sedimentary core (TSR-17-I): chlorophyll derivatives (CD), total carotenes (TC), chlorophyll *a* (chl *a*), pheophytin *a* (phe *a*), chlorophyllide *a*, pheophorbide *a* (pheide *a*) and β-carotene ($\beta\beta$ –car). The ratio between absorbance at 430 nm and at 410 nm, an index of pigment degradation, is also shown. Lithological units C, B and A are indicated from base to top. Historical events are described along units.San Roque reservoir evolution stages (1 and 2) and sub-stages (I, II and III) are indicated (see discussion section).

to 33 cm; AD 1965 to 1985). The multi-proxy analysis makes it possible to infer mesotrophic conditions and incipient eutrophication stage, as shown by lower values of CD and TC than the following sub-stages II and III (Fig. 4).

Sub-stage II is represented by the upper section of UB (33 to 14 cm; AD 1985 to 2005) when the eutrophication became evident, as shown by the increase in several organic proxies related to phytoplankton abundance such as CD (also phe *a* and pheide *a*) and TC (also $\beta\beta$-*car*; Figs. 4 and 5). Black laminated sediments also reflected such conditions. This sub-stage spans from the beginning of the 1980s, when higher nutrient contents promoted phytoplankton growth and eutrophication intensified itself. Historical reports of observed eutrophication at the SRr have been accordingly reported after the second half of the 1970s (Bonetto et al., 1976; García de Emiliani, 1977; Quirós, 1988).

Sub-stage III is recorded within UA and is characterized by a sharp increase in most of the trophic state indicators. This sub-stage begins in the 21st Century and is considered to be a period of intensified eutrophication. Particularly, after AD 2005, OM, C_{tot}, N_{tot} and CD (also shown by chl *a*, phe *a*, pheide *a*, chlorophyllide *a*) show a sharp increase (Figs. 3 and 4). The onset of a hypereutrophic state represents a noticeable change within the centennial SRr's environmental conditions. In agreement with our interpretations, monitoring data from AD 1999 to the present indicate a chronic eutrophication process after ≈ AD 2003 and a shift to a hypereutrophic state following AD 2012 (Rodríguez and Ruiz, 2016).

The sedimentary organic proxies provide evidences that the SRr experienced intense eutrophication as of 1980s. The likely dominant mechanism was through nutrient loading from the surrounding catchment. Urban growth of the littoral city and other main localities at northern SRr catchment area, is reflected in an exponential increase of human population from 1947 to 2010. Population growth shows a thirty-fold increase of the littoral city of Villa Carlos Paz (from 0.2 x· 10^4 to 6.3 x 10^4 inhabitants), displaying the most distinct increase since the 1970s. In addition, the population in the whole SRr catchment presented a fourfold increase (2.2 x 10^4 to 9.4 x 10^4 inhabitants) over the same period (Fig. 7B). The population growth in addition to the lack of an efficient sewage treatment system can be directly related to the recorded increase (sub-stage II) and intensification (sub-stage III) of reservoir eutrophication (Figs. 7B and C). Domestic discharges usually provide nutrients mainly rich in both phosphorus, nitrogen, and organic debris. In this sense, the phosphorus balance during AD 1999-2000 highlights the fact that the diffusive load from littoral areas is the main contribution to the reservoir (61%; Rodríguez and Ruiz, 2016). This fact emphasizes that one of the most important triggers of the increase in eutrophication (sub-stages II and III) is the exponential population growth at the littoral city of Villa Carlos Paz.

In summary, we assume that the population growth (Fig. 7 B) and to a lesser extent changes in the land use within the SRr catchment (Fig. 1B) are the main drivers that caused a threefold increase in the phosphorus load entering the reservoir

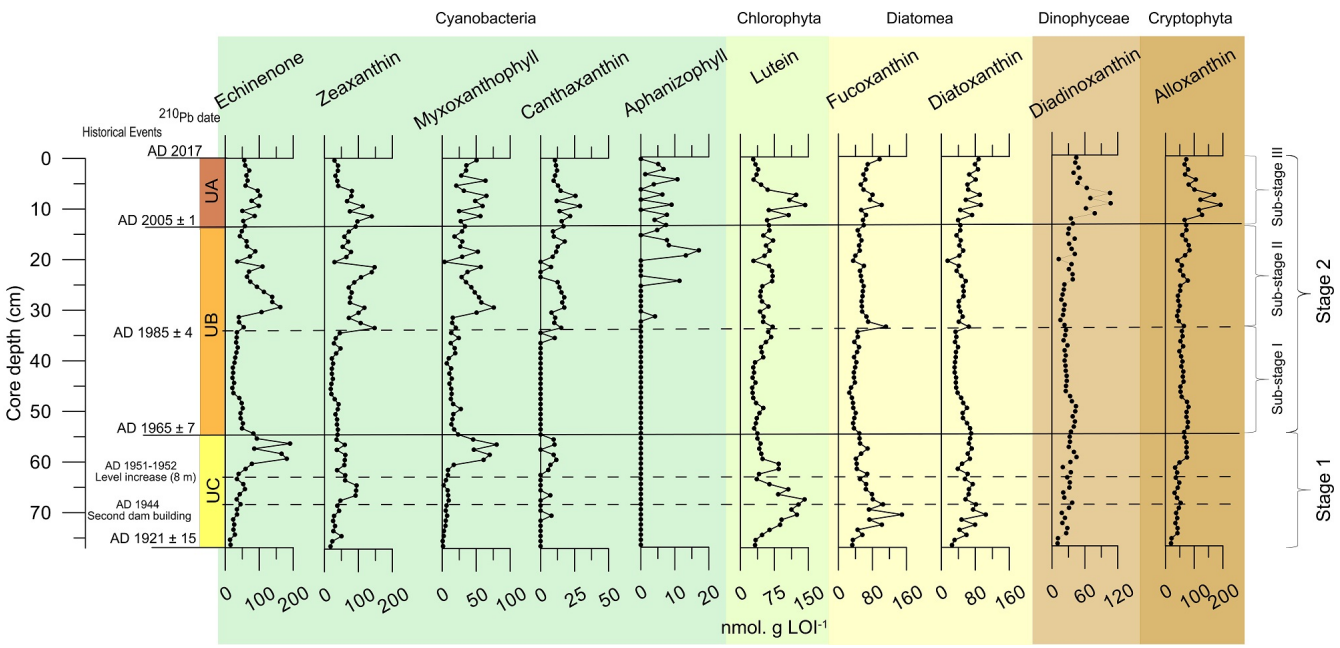

Figure 5. Depth profiles of fossil pigments indicating diverse phytoplankton groups in the SRr sedimentary core (TSR-17-I): echinenone (*echin*), zeaxanthin (*zea*), myxoxanthophyll (*myxo*), canthaxanthin (*cantha*) and aphanizophyll (*apha*): cyanobacteria group (green); lutein (*lut*): chlorophyta group (light green); fucoxanthin (*fuco*) and diatoxanthin (*diato*): diatomea group (yellow); diadinoxanthin (*diadino*): dinophyceae group (light brown); alloxanthin (*allo*): cryptophyta group (brown). Lithological units C, B and A are indicated from base to top. Historical events are described along units.San Roque reservoir evolution stages (1 and 2) and sub-stages (I, II and III) are indicated (see discussion section). (For interpretation of the references to color in this figure legend, the reader is referred to the Web version of this article.)

during the time interval from 1977 (≈ 45 ton·yr^{-1}; Gavilan, 1981) to 2000 (≈ 145 ton·yr^{-1}; Rodríguez and Ruiz, 2016). In addition, forest fires in the SRr catchment can be considered a further factor contributing to the increase of the phosphorus and nitrogen load input into the reservoir (Reyna et al., 2014).

5.2 Fossil Pigments as indicators of reservoir history

Carotene concentration shows the contribution of the different groups of phytoplankton to sedimentary OM during the different reservoir development stages, where Cyanobacteria (*echin*, *zea* and *myxo*), chlorophyta (*lut*) and diatomea (*fuco* and *diato*) are the most representative groups throughout the record (Fig. 5). However, cyanobacteria and dinophyceae seem to mostly contribute to the total biomass as shown by their high correlation with OM and chlorophyll derivatives (Fig. 6). We are aware that some carotenoids differ in their stability, which might lead to an over or underestimation of the abundance of some groups. For example, *fuco* is among the most labile (Turner et al., 2006), so the abundance of diatoms could be underestimated. On the other hand, *allo* should be interpreted with caution because of its selective preservation. Thus, the high peaks of *allo* during the 21st Century could be the result of over-representation in the surface sediments relative to the abundance of cryptophyta (Leavitt, 1993; Reuss et al., 2005). Regarding the environmental evolution in the SRr, we observed several differences in fossil pigments over the inferred stages. The first stage presents high peaks of biomarker pigments of diatoms, chlorophytes and cyanobacteria (Fig. 5). Physical factors, such as fluvial inputs and mixing conditions in aquatic systems promote the dominance of diatoms (Fadel et al., 2015; Visser et al., 2016). Therefore, pigment peaks corresponding to diatom and chlorophyte groups registered over stage 1 (Fig. 5) can be associated to the riverine influence during the initial stage associated to unstable water column mixing conditions. Riverine contribution of diatoms and chlorophytes into the SRr has been reported by previous studies (Guarrera, 1948; Yacubson, 1960). Chlorophyte (*lut*) and diatom (*fuco* and *diato*) markers show a high correlation with mean grain size, as shown by PCA biplot, thus reinforcing the fluvial influence on the abundance of these groups (Fig. 6).

Higher water levels after the construction of the second dam and reservoir infilling probably led to the proliferation of cyanobacteria (*echin*, *zea* and *myxo*; Fig. 5). The onset of more stable conditions could have promoted water column stratification, which is optimum for proliferation of cyanobacteria, as noticed in the SRr (Halac et al., 2019; Rodríguez and Ruiz, 2016). This condition combined with increased nutrient concentrations, low-precipitation periods (mid-1950s until the beginning of the 1970s in Fig. 7A), may have promoted the recorded increase in cyanobacteria pigments from AD 1958

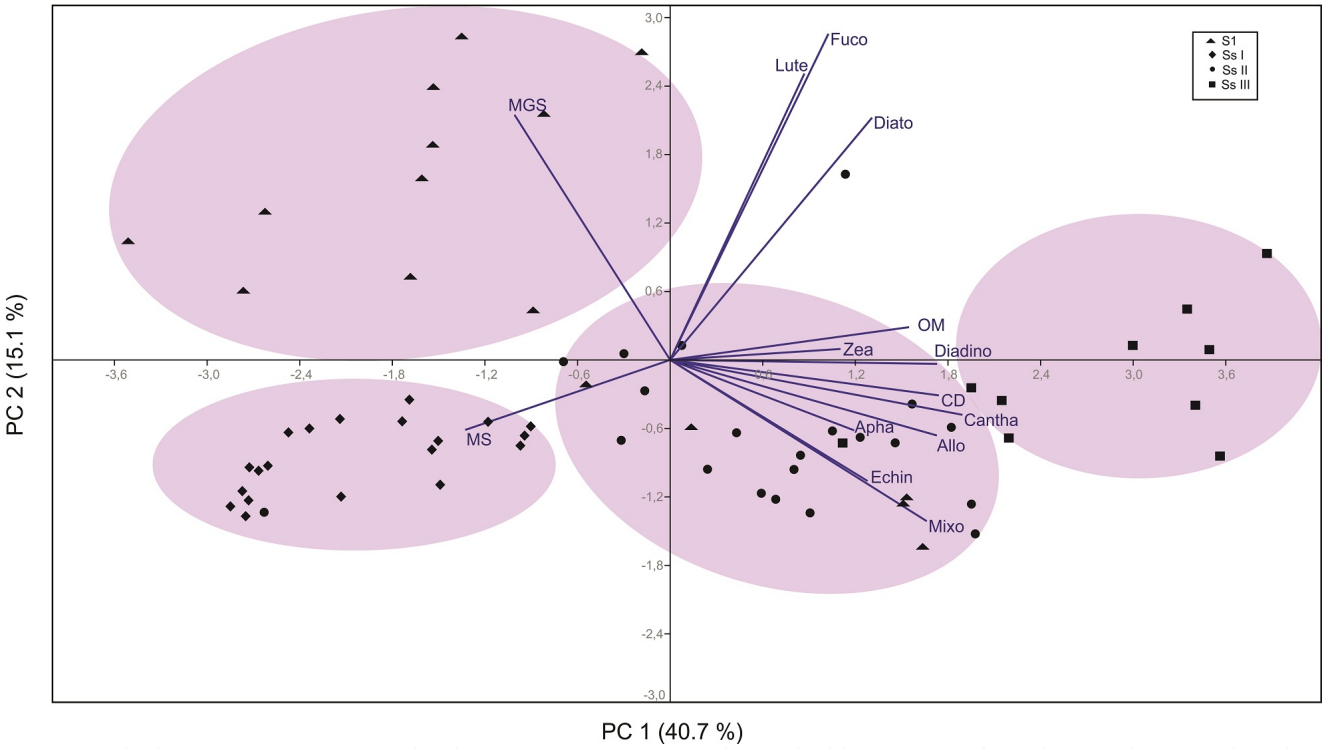

Figure 6. Principal Components Analysis Biplot (Axes 1 and 2) showing variability patterns of physicochemical and biological proxies along the SRr sedimentary record: MGS, mean grain size; MS, magnetic susceptibility; OM, organic matter; CD, chlorophyll derivatives; Echin, echinenone; Zea, zeaxanthin; Myxo, myxoxanthophyll; Cantha, canthaxanthin; Apha, aphanizophyll; Lut, lutein; Fuco, fucoxanthin; Diato, diatoxanthin; Diadino, diadinoxanthin; Allo, alloxanthin. The samples scores are plotted to show the environmental evolution of the SRr: S1: stage 1; Ss I: sub-stage I; Ss II: sub-stage II and Ss III: sub-stage III (see text). Circles indicate the sample groups separated by the first component.

to 1964 (Fig. 7C). The PCA biplot (Fig. 6) shows an opposite ordination of cyanobacteria pigments and mean grain size, this reinforcing favorable conditions for cyanobacteria proliferation.

The second stage, covering the period from AD 1965 to the present, can be split into three sub-stages (I-II-III). Sub-stage I is characterized by the lack of a dominance of a specific phytoplankton group as shown by low marker pigment contents. Over the course of sub-stage II (after AD 1985), the increased eutrophication is revealed by peaks of fossil pigments, especially those from cyanobacteria (*echin*, *zea*, *myxo*). Over the interval AD 1985 to 2000, abundance of cyanobacteria exhibited an increased by three- to fourfold in comparison with the previous sub-stage. Moreover, carotenoid markers of N2–fixing cyanobacteria that displayed either low (*cantha*) or non-detected percentage values (*apha*) before the 1980s, started increasing at sub-stage II (Fig. 5). Hence, the cyanobacteria community structure changes to a major proportion of N2 fixers. Regarding other phytoplankton groups, diatoms (*fuco* and *diato*) and chlorophytes (*lut*) populations show a short-lived response with a distinct peak at by 1985 (Fig. 5).

The high abundance of the cyanobacteria group during sub-stage II suggests that the growth in population and urban development along the SRr catchment after the 1970s impacted on phytoplankton biomass in the SRr (Figs. 7B and C). In accordance with our results, various studies show that periods of major urban growth coincide with cyanobacteria blooms (Pienitz and Vincent, 2003; Winston et al., 2014).

A substantial change in the phytoplankton community structure took place during sub-stage III, which is characterized by the intensification of the eutrophication. Besides cyanobacteria, other groups display a high concentration in marker pigments (Fig. 5). Diatoms (*fuco* and *diato*), dinophytes (*diadino*), chlorophytes (*lut*) and cryptophytes (*allo*) groups show a higher contribution in comparison with previous sub-stages. At the end of sub-stage III, the cyanobacteria group was comparatively less dominant than during sub-stage II, probably due to a marked increase in precipitation as after AD 2013 (Fig. 7A and C; Halac et al., 2019). In agreement with our results, direct monitoring data show similar trends in the different phytoplankton groups over sub-stage III: a) high percentages of diatom contribution throughout sub-stage III; b) an increased concentration of cryptophyte species as after AD 2006 and, c) an increase in the dinophyte abundance and a concomitant decrease in cyanobacteria after AD 2012 to 2016 (Rodríguez and Ruiz, 2016).

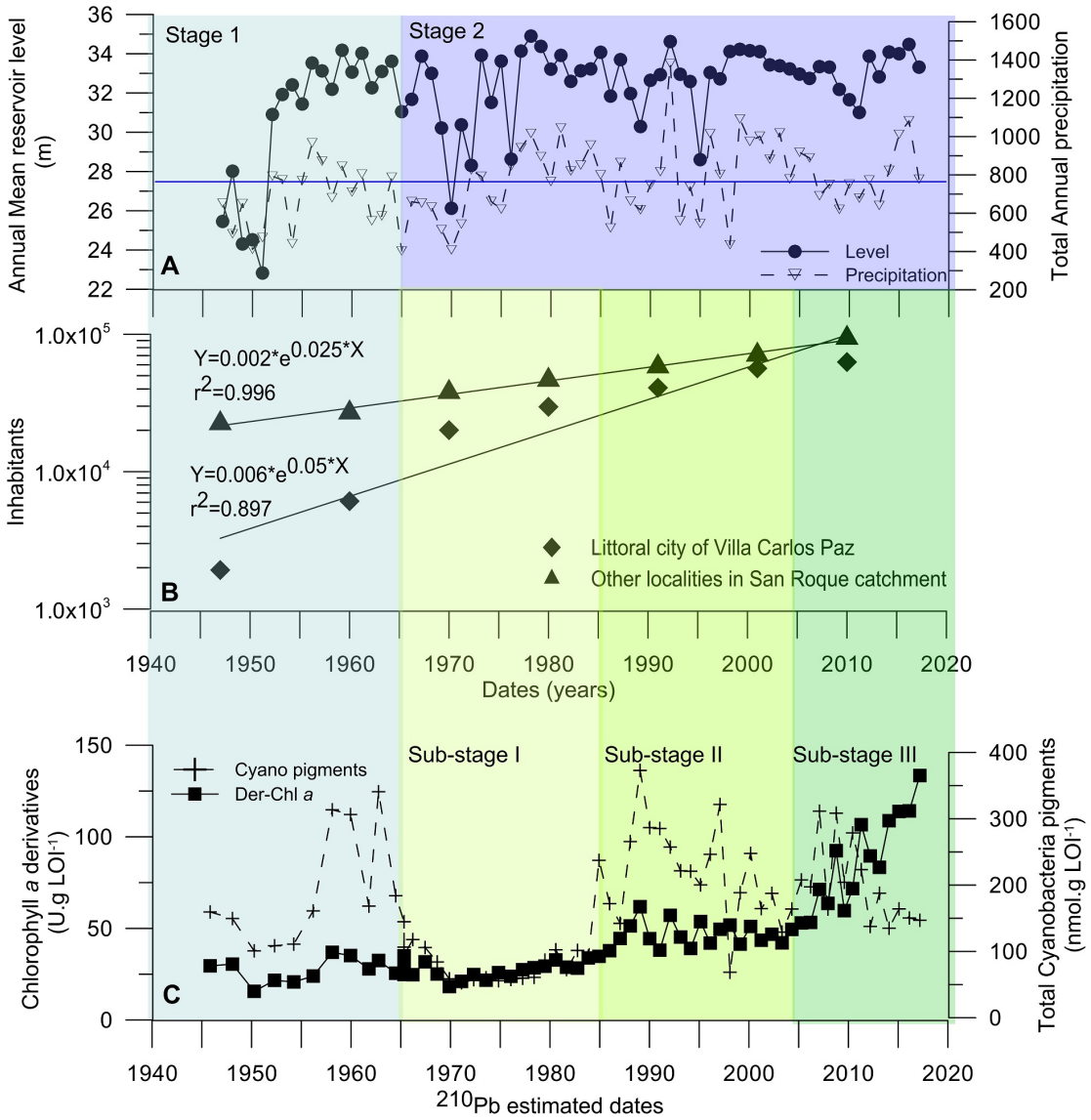

Figure 7. Environmental evolution in the SRr as shown by historical data (A and B; AD 1947 – 2017) and sedimentary record (C; AD 1946 ± 11 – 2017 ± 1). A) Hydrometeorological changes in the San Roque basin: reservoir water level (m) and local total precipitation (mm). The blue line indicates the local mean precipitation value. B) Human population growth at the littoral city of Carlos Paz and at the catchment villages adjusted by an exponential function. C) Chlorophyll derivatives and total cyanobacteria pigment content from sedimentary record. The color bands indicate the different stages and sub-stages. Light blue: stage 1 and blue: stage 2; light green: sub-stage I; green: sub-stage II and dark green: sub-stage III (see text). (For interpretation of the references to color in this figure legend, the reader is referred to the Web version of this article.)

6. Conclusions

The use of fossil pigments provided important clues to decipher the physical and trophic state history of the SRr prior to the water quality monitoring survey. The temporal variability in physicochemical and biological proxies along with instrumental data, reveal that nutrient input, fluvial influence and hydrometeorological factors are the main drivers for the environmental change of the SRr. Overall the SRr environmental history we identified: 1. An initial period dominated by biological responses mainly ruled by fluvial processes; 2. A shift to predominantly inner-lake sedimentary conditions due to changes in the base level; 3. A triggering in the eutrophication processes since the 1980s related to population growth in the catchment and littoral areas; 4. Predominance of the cyanobacteria group as the main response to the eutrophication process; and 5. The influence of hydrometeorological factors, such as water level and/or precipitation variability, as additional forces affecting the composition of the phytoplankton community.

Paleolimnological studies in reservoirs on the environmental response to temporal land-use changes along with an un-

derstanding of climatic forces are fundamental in defining background conditions and providing data to predict future scenarios. Further research considering paleolimnological data calibrated with water quality monitoring is needed to obtain more precise reconstructions. Paleolimnological reconstructions combined with continuous monitoring contribute to broadening the time framework of the analyses. This approach is essential to be able to assess water management strategies effectively.

Acknowledgments

This work was supported by Agencia Nacional de Promoción Científica y Tecnológica (PICT-2013-1371 and PICT-2014-3298), Consejo Nacional de Investigaciones Científicas y Técnicas (PUE-2016-CICTERRA), Secretaría de Ciencia y Técnica - Universidad Nacional de Córdoba (PRIMAR-TP-2018-32520170100051CB-UNC and SECYT- CONSOLIDAR- 2018-411-18). Support was provided to L.M. by a grant from CONICET (Argentina) and to L.G. by a grant from the Federal Commission for Scholarships for Foreign Students FCS (2017-2018).We would like to thank Dirección de Seguridad Náutica (Córdoba, Argentina) for supporting the fieldwork and to Instituto Nacional del Agua - Centro de la Región Semiárida for providing water quality monitoring data. We also thank the comments and suggestions of the Editor and two anonymous reviewers, which helped improve the manuscript.

References

Appleby, P.G., 2001. Chronostratigraphic Techniques in Recent Sediments, in: Last, W.M., Smol, J.P. (Eds.), Tracking Environmental Change Using Lake Sediments. Volume 1: Basin Analysis, Coring and Chronological Techniques. KluwerAcademic Publishers Dordrecht, pp. 171–203.

Ballester, R., 1931. Proyecto del nuevo Dique San Roque. Rev. la Univ. Nac. Córdoba 18, 42–65. [Project of the new San Roque Dam].

Bartram, J., Ballance, R. (Eds.), 1996. Water quality monitoring: a practical guide to the design and implementation of freshwater quality studies and monitoring programmes. United Nations Environment Programme and the World Health Organization (UNEP/WHO).

Birks, H.H., Birks, H.J.B., 2006. Multi-proxy studies in palaeolimnology. Veg. Hist. Archaeobot. 15, 235–251. https://doi.org/10.1007/s00334-006-0066-6.

Blott, S.J., Pye, K., 2001. GRADISTAT: A grain size distribution and statistics package for the analysis of unconsolidated sediments. Earth Surf. Process. Landforms 26, 1237–1248. https://doi.org/10.1016/S0167-5648(08)70015-7.

Bonetto, A.A., Di Persia, D.H., Maglianesi, R., Corigliano, M. del C., 1976. Caracteres limnológicos de algunos lagos eutróficos de embalse de la Región Central de Argentina. ECOSUR 3, 83–98. [Limnological characters of some eutrophic reservoirs in the Central Region of Argentina].

Bradbury, J.P., Van Metre, P.C., 1997. A land-use and water-quality history of White Rock Lake Reservoir, Dallas, Texas, based on paleolimnological analyses. J. Paleolimnol. 17, 227–237. https://doi.org/10.1023/A:1007923829759.

Buchaca, T., Catalan, J., 2007. Factors influencing the variability of pigments in the surface sediments of mountain lakes. Freshw. Biol. 52, 1365–1379. https://doi.org/10.1111/j.1365-2427.2007.01774.x.

Catalini, C.G., García, C.M., 2014. Análisis estadístico descriptivo sobre series hidrológicas del Embalse San Roque (período 1947-2009). https://www.ucc.edu.ar/portalucc/ archivos/File/ Ingenieria/Grupos_Investigacion/EHCPA/2010/analisisserieshidrologicasembalse sanroque.pdf [Descriptive statistical analysis on historic hydrological series of San Roque reservoir (period 1947-2009)].

Coianiz, L., Ariztegui, D., Piovano, E.L., Lami, A., Guilizzoni, P., Gerli, S., Waldmann, N., 2014. Environmental change in subtropical South America for the last two millennia as shown by lacustrine pigments. J. Paleolimnol. 53, 233–250. https://doi.org/10.1007/s10933-014-9822-2.

Colladón, L., 2014. Síntesis pluviométrica 1992-2012, Cuenca del río San Antonio: Sistema del Río Suquía, Provincia de Córdoba. Instituto Nacional del Agua, Ezeiza https://www.ina.gov.ar/legacy/pdf/CIRSA_ Sintesis _1992_2012 _ISBN.pdf [Rainfall Synthesis 1992-2012, San Antonio River Basin: Suquía River System, Province of Córdoba].

Costa-Böddeker, S., Bennion, H., Araújo de Jesus, T., Albuquerque, A.L.S., Figueira, R.C.L., Bicudo, D. de C., 2012. Paleolimnologically inferred eutrophication of a shallow , tropical, urban reservoir in southeast Brazil. J. Paleolimnol. 751–766. https://doi.org/10.1007/s10933-012-9642-1.

Dasso, C.M., Piovano, E.L., Pasquini, A.I., Córdoba, F.E., 2014. Recursos hídricos superficiales. Relat. del XIX Congr. Geológico Argentino 1209–1231. [Surface water resources].

Dean, W.E., 1974. Determination of carbonate and organic matter in calcareous sediments and sedimentary rocks by loss of ignition: comparison with other methods. J. Sediment. Petrol. 44, 242–248.

Díaz, E., Corral, M., Lábaque, M., Vicario, L., Pozzi Piacenza, C., Moya, G., García, M., Tarrab, L., Rodríguez, A., 2016. Hydrology and hydraulics of the Suquía River Basin, in: Wunderlin, D.A. (Ed.), The Suquía River Basin (Córdoba, Argentina). The Handbook of Environmental Chemistry. Springer, Cham, pp. 1–35.

Egeland, E.S., Garrido, J.L., Clementson, L., Andresen, K., Thomas, C.S., Zapata, M., Airs, R., LLewellyn, C.A., Newman, G.L., Rodrıguez, F., Roy, Suzanne,

2011. Data sheets aiding identification of phytoplankton carotenoids and chlorophylls in collaboration with, in: Roy, S., Llewellyn, C., Egeland, E., Johnsen, G. (Eds.), Phytoplankton Pigments: Characterization, Che motaxonomy and Applications in Oceanography. Cambridge University Press, Cambridge, UK, pp. 665–822.

Fadel, A., Atoui, A., Lemaire, B.J., Vinçon-Leite, B., Slim, K., 2015. Environmental factors associated with phytoplankton succession in a Mediterranean reservoir with a highly fluctuating water level. Environ. Monit. Assess. 187. https://doi.org/10.1007/s10661-015-4852-4.

Fontana, L., Albuquerque, A.L.S., Brenner, M., Bonotto, D.M., Sabaris, T.P.P., Pires, M.A.F., Cotrim, M.E.B., Bicudo, D. de C., 2014. The eutrophication history of a tropical water supply reservoir in Brazil. J. Paleolimnol. 51, 29–43. https://doi.org/10.1007/s10933-013-9753-3.

Gangi, D., Plastani, M.S., Laprida, C., Lami, A., Dubois, N., Bordet, F., Gogorza, C., Frau, D., de Tezanos Pinto, P., 2020. Recent cyanobacteria abundance in a large subtropical reservoir inferred from analysis of sediment cores. J. Paleolimnol. 63, 195–209. https://doi.org/10.1007/s10933-020-00110-8.

García de Emiliani, M.O., 1977. Ciclo anual del fitoplancton en el Embalse San Roque (Córdoba, Argentina). Rev. Asoc. Ciencias Nat. Litoral 8, 1–12. [Annual cycle of phytoplankton in the San Roque Reservoir (Córdoba, Argentina)].

Gavilan J.G., 1981. Study water quality in the san Roque reservoir. Water Qual. Bull. Environ. 6 (4), 136–158.

Gilbert, R.O., 1987. Statistical methods for environmental pollution monitoring. John Wiley and Sons, New York.

Granero, M., Bustamante, A., López, F., Ruiz, M., 2004. Hipolimnion water quality and its relationship to internal P loading in an eutrophicated water body: San Roque Reservoir (Córdoba, Argentina). J. Hydraul. Res. 42, 310–315. https://doi.org/10.1080/00221686.2004.9728396.

Guarrera, S.A., 1948. El fitoplancton del Embalse San Roque (Provincia de Cordoba). Rev. del Inst. Nac. Investig. las Ciencias Nat. anexo al Mus. Ciencias Nat. "Bernadino Rivadavia" 1, 29–55. [The phytoplankton of San Roque Reservoir (Province of Cordoba)].

Guerra, L., Piovano, E.L., Córdoba, F.E., Tachikawa, K., Rostek, F., Garcia, M., Bard, E., Sylvestre, F., 2017. Climate change evidences from the end of the Little Ice Age to the Current Warm Period registered by Melincué Lake (Northern Pampas, Argentina). Quat. Int. 438, 160–174. https://doi.org/10.1016/j.quaint.2016.06.033.

Guilizzoni, P., Bonomi, G., Galanti, G., Ruggiu, D., 1983. Relationship between sedimentary pigments and primary production: evidence from core analyses of twelve Italian lakes. Hydrobiologia 103, 103–106. https://doi.org/10.1007/BF00028436.

Guilizzoni, P., Lami, A., 2003. Paleolimnology: use of algal pigments as indicators, in: Bitton, G. (Ed.), Encyclopedia of Enviromental Microbiology. Wiley and Sons, Chichester, pp. 2306–2317.

Halac, S., Bazán, R., Larrosa, N., Nadal, A.F., Ruibal Conti, A.L., Rodríguez, M.I., Ruiz, M., Lopéz, A.G., 2019. First report on negative association between cyanobacteria and fecal indicator bacteria at San Roque reservoir (Argentina): impact of environmental factors. J. Freshw. Ecol. 34, 273–291. https://doi.org/10.1080/02705060.2019.1595752.

Heiri, O., Lotter, A.F., Lemcke, G., 2001. Loss on ignition as a method for estimating organic and carbonate content in sediments: reproducibility and comparability of results. J. Paleolimnol. 25, 101–110.

Hodgson, D.A., Vyverman, W. V., Verleyen, E., Sabbe, K., Leavitt, P.R., Taton, A., Squier, A.H., Keely, B.J., 2004. Environmental factors influencing the pigment composition of in situ benthic microbial communities in east Antarctic lakes. Aquat. Microb. Ecol. 37, 247–263. https://doi.org/10.3354/ame037247.

Huo, S., Zhang, H., Ma, C., Xi, B., Zhang, J., He, Z., Li, X., Wu, F., 2019. Algae community response to climate change and nutrient loading recorded by sedimentary phytoplankton pigments in the Changtan Reservoir, China. J. Hydrol. 571, 311–321. https://doi.org/10.1016/j.jhydrol.2019.02.005.

Lami, A., Niessen, F., Guilizzoni, P., Masaferro, J., Belis, C.A., 1994. Palaeolimnological studies of the eutrophication of volcanic Lake Albano (Central Italy). J. Paleolimnol. 10, 181–197. https://doi.org/10.1007/BF00684032.

Lami, A., Guilizzoni, P., Marchetto, A., 2000. High resolution analysis of fossil pigments, carbon, nitrogen and sulphur in the sediment of eight European Alpine lakes: The MOLAR project. J. Limnol. 59, 15–28. https://doi.org/10.4081/jlimnol.2000.s1.15.

Lami, A., Turner, S., Musazzi, S., Gerli, S., Guilizzoni, P., Rose, N.L., Yang, H., Wu, G., Yang, R., 2010. Sedimentary evidence for recent increases in production in Tibetan plateau lakes. Hydrobiologia 648, 175–187. https://doi.org/10.1007/s10750-010-0263-2.

Leavitt, P.R., 1993. A review of factors that regulate carotenoid and chlorophyll deposition and fossil pigment abundance. J. Paleolimnol. 9, 109–127.

Leavitt, P.R., Hodgson, D.A., 2001. Sedimentary Pigments, in: Tracking Environmental Change Using Lake Sediments. KluwerAcademic Publishers Dordrecht, pp. 295–325. https://doi.org/10.1007/0-306-47668-1.

Leslie, C., Hancock, G.J., 2008. Estimating the date corresponding to the horizon of the first detection of ^{137}Cs and $^{239+240}$Pu in sediment cores. J. Environ. Radioact. 99, 483–490. https://doi.org/10.1016/j.jenvrad.2007.08.016.

McLeod, A.I., 2011.Package 'Kendall' R Package. version 2.2.

Moss, B., 1967. Percentage degradation of chlorophylls to pheo-pigments. Limnol. Oceanogr. 12, 335–340.

O'Farrell, I., Motta, C., Forastier, M., Polla, W., Otaño, S., Meichtry, N., Lombardo, R., 2019. Ecological meta-analysis of bloom-forming planktonic Cyanobacteria in

Argentina. Harmful algae, 83, 1–13. https://doi.org/10.1016/j.hal.2019.01.004.

O'Neil, J.M., Davis, T.W., Burford, M.A., Gobler, C.J., 2012. The rise of harmful cyanobacteria blooms: The potential roles of eutrophication and climate change. Harmful Algae 14, 313–334. https://doi.org/10.1016/j.hal.2011.10.027.

Oksanen, J., F. Guillaume Blanchet, R.K., Legendre, P., Minchin, P.R., O'Hara, R.B., Simpson, G.L., Solymos, P., M. Henry H. Stevens, H.W., 2019. Package 'vegan.' R Packag. version 3.4.0.

Paerl, H.W., Huisman, J., 2008. Blooms like it hot. Science 320, 57–58.

Paerl, H.W., Paul, V.J., 2012. Climate change : Links to global expansion of harmful cyanobacteria. Water Res. 46, 1349–1363. https://doi.org/10.1016/j.watres.2011.08.002.

Pasquini, A.I., Lecomte, K.L., Piovano, E.L., Depetris, P.J., 2006. Recent rainfall and runoff variability in central Argentina. Quat. Int. 158, 127–139. https://doi.org/10.1016/j.quaint.2006.05.021.

Pennington, W., Tutin, T.G., Cambray, R.S., Fisher, E.M., 1973. Observations on lake sediments using fallout 137Cs as a tracer. Nature 242, 20. https://doi.org/10.1038/246421a0.

Pienitz, R., Vincent, W.F., 2003. Generic approaches towards water quality monitoring based on paleolimnology, in: Kumagai, M., Vincent, W.F. (Eds.), Freshwater Management: Global versus Local Perspectives. Springer-Verlag, Tokyo, pp. 61–82.

Piovano, E.L., Córdoba, F.E., Stutz, S., 2014. Limnogeology in Southern South America: An overview. Lat. Am. J. Sedimentol. Basin Anal. 21, 65–75.

Pizzolon, L., Tracanna, B., Prósperi, C., Guerrero, J.M., 1999. Cyanobacterial blooms in Argentinean inland waters. Lakes Reserv. Res. Manag. 4, 101–105.

Quirós, R., 1988. Relationships between air temperature, depth, nutrients and chlorophyll in 103 Argentinian lakes. Verh. Internat. Verein. Limnol 23, 647–658.

Reuss, N., Conley, D.J., Bianchi, T.S., 2005. Preservation conditions and the use of sediment pigments as a tool for recent ecological reconstruction in four Northern European estuaries. Mar. Chem. 95, 283–302. https://doi.org/10.1016/j.marchem.2004.10.002.

Reyna, S., Reyna, T., La, M., 2014. Fire Impacts to Quality of Reservoirs San Roque and Los Molinos. Pinnacle Environ. Earth Sci. 1, 1–7.

Robbins, J.A., 1978. The biogeochemistry of lead in the environment. Edited by JO Nriagu, 285.

Rodríguez, M.I., Ruiz, M., 2016. Limnology of the San Roque Reservoir, in: Wunderlin, D. (Ed.), The Suquía River Basin (Córdoba, Argentina). The Handbook of Environmental Chemistry. Springer, Cham, pp. 37–59. https://doi.org/10.1007/698.

Romero-Viana, L., Keely, B.J., Camacho, A., Vicente, E., Rosa Miracle, M., 2009. Photoautotrophic community changes in Lagunillo del Tejo (Spain) in response to lake level fluctuation: Two centuries of sedimentary pigment records. Org. Geochem. 40, 376–386. https://doi.org/10.1016/j.orggeochem.2008.11.010.

Sánchez-Cabeza, J.A., Ruiz-Fernández, A. C. (2012). 210Pb sediment radiochronology: an integrated formulation and classification of dating models. Geochimica et Cosmochimica Acta 82, 183–200.

Shotbolt, L.A., Hutchinson, S.M., Thomas, A.D., 2006. Sediment stratigraphy and heavy metal fluxes to reservoirs in the southern Pennine uplands, UK. J. Paleolimnol. 35, 305–322. https://doi.org/10.1007/s10933-005-1594-2.

Sima, O., Arnold, D., Dovlete, C., 2001. GESPECOR: A versatile tool in gamma-ray spectrometry. J. Radioanal. Nucl. Chem. 248, 359–364.

Smith, V.H., 2003. Eutrophication of freshwater and coastal marine ecosystems: A global problem. Environ. Sci. Pollut. Res. 10, 126–139. https://doi.org/10.1065/espr2002.12.142.

Smith, V.H., Schindler, D.W., 2009. Eutrophication science: where do we go from here? Trends Ecol. Evol. 24, 201–207. https://doi.org/10.1016/j.tree.2008.11.009.

Smol, J.P., 2010. The power of the past: Using sediments to track the effects of multiple stressors on lake ecosystems. Freshw. Biol. 55, 43–59. https://doi.org/10.1111/j.1365-2427.2009.02373.x.

ter Braak, C.J.F., 1995. Data analysis in community and landscape ecology. Cambridge University Press. https://doi.org/10.1177/001452461602701106.

Tremblay, R., Légaré, S., Pienitz, R., Vincent, W.F., Hall, R.I., 2001. Paleolimnological analysis of changes in the trophic status of Lake Saint-Charles, a drinking water reservoir for the Québec urban community. Rev. des Sci. L'eau 14, 489–510.

Turner, R.E., Rabalais, N.N., Fry, B., Atilla, N., Milan, C.S., Lee, J.M., Normandeau, C., Oswald, T.A., Swenson, E.M., Tomasko, D.A., 2006. Paleo-indicators and water quality change in the Charlotte Harbor estuary (Florida). Limnol. Oceanogr. 51, 518–533. https://doi.org/10.4319/lo.2006.51.1_part_2.0518.

UNSCEAR, 2000. Exposures from man-made sources of radiation. Report volume 1: sources, annex C.

Vicario, L., 2017. Identificación y evaluación de sequías en cuencas seleccionadas de la Región Centro de Argentina. Ph.D. Thesis, Universidad Nacional de Córdoba. https://rdu.unc.edu.ar/bitstream/handle/11086/6291/Tesis%20Doctoral%20Leticia%20VICARIO.pdf. [Identification and evaluation of drought in selected basins of the central region of Argentina].

Visser, P.M., Ibelings, B.W., Bormans, M., Huisman, J., 2016. Artificial mixing to control cyanobacterial blooms: a review. Aquat. Ecol. 50, 423–441. https://doi.org/10.1007/s10452-015-9537-0.

Vörösmarty, C.J., McIntyre, P.B., Gessner, M.O., Dudgeon, D., Prusevich, A., Green, P., Glidden, S., Bunn, S.E., Sullivan, C.A., Liermann, C.R., Davies, P.M., 2010.

Global threats to human water security and river biodiversity. Nature 467, 555–561. https://doi.org/10.1038/nature09440.

Winston, B., Hausmann, S., Escobar, J., Kenney, W.F., 2014. A sediment record of trophic state change in an Arkansas (USA) reservoir. J. Paleolimnol. 51, 393–403. https://doi.org/10.1007/s10933-013-9762-2.

Yacubson, S., 1960. Desmidiáceas del Lago San Roque y tributarios (provincia de Córdoba, Argentina). Boletín la Soc. Argentina Botánica 8, 63–89. [Desmidiaceae of Lake San Roque and tributaries (province of Córdoba, Argentina)].

Züllig, H., 1985. Carotenoids from plankton and purple sulphur bacteria in lake sediments as indicators of changes in the environment. Experientia 41, 533–534.

Züllig, H., 1982. Untersuchungen über die Stratigraphie von Carotinoiden im geschichteten Sediment von 10 Schweizer Seen zur Erkundung früherer Phytoplankton-Entfaltungen. Schweizerische Zeitschrift für Hydrol. 44, 1–98. https://doi.org/10.1007/BF02502191.

https://datosestadistica.cba.gov.ar/dataset/censo- 2010-resultados-definitivos. Date of last access: June 9th 2020.

https://datosestadistica.cba.gov.ar/dataset/sector-turismo. Date of last access: June 9th 2020.

http://lrc.geo.umn.edu/laccore/icd.html. Date of last access: June 9th 2020.

Table A1. Principal marker pigments, relative taxa and acronym list.

Acronym	**Pigment**	**Taxa**
	Chlorophylls	
Chl *a*	Chlorophyll *a*	common to all plants
Chl *b*	Chlorophyll *b*	Chlorophyta, Euglenophyta
Chl c	Chlorophyll *c*	Chrysophyta, Dinophyceae
	Chlorophyll derivatives	
Pheide_*a*	Pheophorbides *a*	chlorophyll *a* derivative (grazing)
Phe_*a*	Pheophythin *a*	chlorophyll *a* derivative common to all plants
Phe_*b*	Pheophythin *b*	chlorophyll *b* derivative common to all plants
Phe_*c*	Pheophythin *c*	chlorophyll *c* derivative (Chrysophyta, Dinophyceae)
	Carotenes	
$\beta\beta$_car	$\beta;\beta$-carotene	common to all plants, some bacteria, Chlorophyta
	Xanthophylls	
Allo	Alloxanthin	Cryptophyta
Cantha	Canthaxanthin	Invertebrate herbivores, some filamentous Cyanobacteria
Echin	Echinenone	Total Cyanobacteria
Zea	Zeaxanthin	Total Cyanobacteria
Myxo	Myxoxanthophyll	Colonial and filamentous Cyanobacteria
Apha	Aphanizophyll	N_2-fixing Cyanobacteria
Fuco	Fucoxanthin	Siliceous algae (including Diatomea)
Diato	Diatoxanthin	Diatomea
Lut	Lutein	Chlorophyta, Euglenophyta
Diadino	Diadinoxanthin	Dinophyceae, Euglenophyta